Demonstration of a quantum advantage by a joint detection receiver for optical communication using quantum belief propagation on a trapped-ion device

Conor Delaney,[1] Kaushik P. Seshadreesan,[2,3,*] Ian MacCormack,[1,4,5] Alexey Galda,[6] Saikat Guha,[2] and Prineha Narang[7,†]

[1]*Aliro Technologies, Inc., Boston, Massachusetts 02135, USA*
[2]*College of Optical Sciences, The University of Arizona, Tucson, Arizona 85721, USA*
[3]*School of Computing and Information, University of Pittsburgh, Pittsburgh, Pennsylvania 15260, USA*
[4]*Kadanoff Center for Theoretical Physics, University of Chicago, Chicago, Illinois 60637, USA*
[5]*Department of Physics, Princeton University, Princeton, New Jersey 08544, USA*
[6]*James Franck Institute, University of Chicago, Chicago, Illinois 60637, USA*
[7]*School of Engineering and Applied Sciences, Harvard University, Cambridge, Massachusetts 02138, USA*

(Received 11 January 2022; accepted 7 July 2022; published 28 September 2022)

Demonstrations of quantum advantage have largely focused on computational speedups and on quantum simulation of many-body physics, limited by fidelity and the capability of current devices. Discriminating laser-pulse-modulated classical-communication code words at the minimum allowable probability of error using universal-quantum processing presents a promising parallel direction, one that is of both fundamental importance in quantum state discrimination and technological relevance in deep-space laser communications. Here we present an experimental realization of a quantum joint detection receiver for binary phase shift keying modulated code words of a 3-bit linear tree code using a recently proposed quantum algorithm: belief propagation with quantum messages. The receiver, translated to a quantum circuit, was experimentally implemented on a trapped-ion device—the recently released Honeywell LT-1.0 system using $^{171}Yb^{+}$ ions, which possesses all-to-all connectivity and midcircuit measurement capabilities that are essential to this demonstration. We conclusively realize a previously postulated but hitherto not demonstrated joint quantum detection scheme and provide an experimental framework that surpasses the quantum limit on the minimum average decoding error probability associated with pulse-by-pulse detection in the low-mean-photon-number limit. The full joint detection scheme bridges across photonic and trapped-ion-based quantum information science, mapping the photonic coherent states of the modulation alphabet onto inner product-preserving states of single-ion qubits. Looking ahead, our work opens new avenues in hybrid realizations of quantum-enhanced receivers with applications in astronomy and emerging space-based platforms.

DOI: 10.1103/PhysRevA.106.032613

I. INTRODUCTION

Optical laser communication is a critical component of future space-based data communications [1]. It offers significantly higher communication rates compared to traditional radio-frequency systems, with lower size, weight, and transmission power requirements [2]. An ideal laser pulse is quantum mechanically described by a *coherent state* $|\alpha\rangle$ of a spatiotemporal-polarization mode of the quantized electromagnetic field, where $|\alpha|^2$ is the mean photon number [3]. Any two coherent states $|\alpha\rangle$ and $|\beta\rangle$ of a mode are known to be nonorthogonal; that is, their inner product $\sigma \equiv \langle\alpha|\beta\rangle = \exp[-(|\alpha|^2 + |\beta|^2 - 2\alpha\beta^*)/2] \neq 0$, which fundamentally precludes error-free discrimination of the states [4]. The minimum achievable probability of error of distinguishing the above two states (assuming they are equally likely to occur) by a physically realizable receiver as imposed by the laws of quantum mechanics, the so-called *Helstrom limit*, is $P_{e,\min} = \frac{1}{2}[1 - \sqrt{1 - |\sigma|^2}] = \frac{1}{2}[1 - \sqrt{1 - e^{-|\alpha-\beta|^2}}]$. This minimum probability of error is, in principle, attainable *exactly* by the all-photonic receiver proposed by Dolinar [5], which employs a coherent-state local oscillator (LO), a beam splitter, a shot-noise-limited photon detector, and an electro-optic feedback from the detector output to drive an electro-optic modulator that controls the amplitude and phase of the LO. Each of these components is readily realizable in a modern optics laboratory. In the context of discriminating more than two coherent states, e.g., discriminating $\{|-\alpha\rangle, |0\rangle, |\alpha\rangle\}$, or discriminating more than two coherent-state *code words*, e.g., $\{|-\alpha\rangle|\alpha\rangle|-\alpha\rangle|\alpha\rangle, |\alpha\rangle|\alpha\rangle|\alpha\rangle|-\alpha\rangle, |\alpha\rangle|-\alpha\rangle|\alpha\rangle|-\alpha\rangle\}$, a Dolinar-like all-photonic receiver is not known to achieve the Helstrom limit. There has been a large body of recent work on feedback-based optical receivers for M-ary coherent-state discrimination [6–9]—building upon the "conditional nulling" receiver designs for M-ary coherent-state pulse-position-modulation [10,11] and phase-shift-keying (PSK) [12] alphabets—whose achievable error probability performance was shown to approach the Helstrom limit in the limit of a *high* mean photon number of the candidate states. In long-range transmissions, photon loss

*kausesh@pitt.edu
†prineha@seas.harvard.edu

renders the laser communication signals increasingly weak with distance. This attenuation causes the coherent states of the modulation alphabet to become highly nonorthogonal, making it nearly impossible to perfectly demodulate coherent-state code words, thereby posing a critical challenge to communicating reliably at a good rate with the distance of the channel. In this regime of low mean photon number per mode at the receiver, a receiver that employs a quantum joint detection measurement on the entire code word can attain the Helstrom limit of minimum error discrimination of code words, and there emerges a large gap in the reliable communication rate achievable with a quantum joint detection receiver (one that would require a true universal-capable quantum processor or computer) versus that achievable with conventional receivers, such as single-photon detectors (even if such a conventional receiver is assumed to be operating at its quantum-mechanics-mandated noise limit). Furthermore, no known all-photonic receiver design can attain the multihypothesis coherent-state Helstrom limit in this aforesaid regime. However, it is known that if each individual coherent state of the modulation alphabet comprising the received code word is *transduced* into a qubit register one by one while maintaining their relative inner product σ (hence their quantum-mandated distinguishability), followed by quantum computing on that multiqubit register, one can achieve the Helstrom limit of telling apart any set of $M \geqslant 2$ coherent-state code words exactly [13].

Fundamental limits on the rate of reliable classical communication over a quantum channel with a modulation alphabet consisting of highly nonorthogonal quantum states is given by the Holevo-Schumacher-Westmoreland theorem [14,15], often termed the "Holevo capacity" C, measured in bits per channel use. For an optical channel with photon loss and thermal noise, each "use" of which can be considered to be the transmission of a single spatiotemporal-polarization mode of light under a mean-photon-number constraint at the transmitter, coherent-state modulation is known to attain the Holevo capacity [16,17]. For any given coherent-state-modulation alphabet, the structure of the optical receiver governs the achievable reliable communication rate, given by the Shannon capacity associated with a particular receiver. Even though the receiver's job is to tell apart a set of $M = 2^{nR}$ product *code words*, each being a product state of n coherent states, there is a fundamental gap between the decoding performance achievable with a receiver that detects each received modulated coherent state in the code word one at a time and a receiver that collectively detects the entire code word using a quantum-enabled processor, thus representing a provable *quantum advantage* scenario. A specific realization of such a joint detection receiver would involve optical domain quantum preprocessing of the modulated code word prior to detection [6,18–20]. This gap can be quantified in terms of the communication capacity and the average decoding error probability associated with the two types of receivers and has been shown theoretically [16,18,21–23] and verified experimentally [6,7]. With a receiver that attains the Holevo capacity, the average probability of error in discriminating the $M = 2^{nR}$ code words can be made to approach zero, as n increases, as long the rate of the code $R < C$.

II. FIDELITY-LIMITED JOINT DETECTION SCHEMES

Recently, a structured design of a quantum joint detection receiver based on an algorithm known as belief propagation with quantum messages (BPQM) [24] was proposed to discriminate binary PSK (BPSK)-modulated coherent-state code words of an exemplary 5-bit linear tree code. It was shown not only to surpass the performance of the best possible conventional receiver that detects the received coherent-state pulses one at a time but also to attain the quantum limit on the minimum average decoding error probability [25,26], the code-word Helstrom limit. The design of the receiver readily translates into a low-depth quantum circuit realizable on current quantum devices, which are designed for complex algorithms [27–32]. We specifically realize sections of joint detection receiver circuitry on Honeywell's LT-1.0 trapped-ion processor, leveraging all-to-all gate connectivity and midcircuit measurements. The necessity of these midcircuit measurements, currently not viable on superconducting quantum devices, makes trapped-ion processors the ideal platform for this demonstration. We also propose a concrete transduction mechanism to couple the states $\{|\alpha\rangle, |-\alpha\rangle\}$ of the BPSK alphabet to (one of two states of) a single trapped-ion qubit. Although the coupling is not physically realized, when coupling inefficiencies are accounted for in the realization of the joint detection receiver circuitry, it still demonstrates a fundamentally improved performance in the decoding error probability achievable over *any* receiver that demodulates the BPSK pulses in the code-word blocks one at a time. This includes all conventional optical receivers such as homodyne detection, heterodyne detection, and direct detection receivers (for example, superconducting nanowire single-photon detectors), as well as the Dolinar receiver [5].

Realization of a true joint detection receiver in the near-term requires heterogeneous quantum hardware, namely, trapped-ion and photonic systems, in coupling with theoretical efforts to map across them [33,34]. The ability to perform the BPQM decoding algorithm, which effects a joint measurement to distinguish the photonically encoded messages, is a single step in the overall scheme. The general overview of the scheme is presented in Fig. 1(a), which shows a long-distance photonic communication being received and decoded. The receiver here requires a method for transduction from the photonic information domain into the trapped-ion quantum device, as well as quantum hardware with minimal noise to run the decoding efficiently and reliably. In this work we focus on the use of trapped-ion devices, specifically the Honeywell LT-1.0 system, although in theory this could be realized with any quantum computer with low enough noise and the ability to perform midcircuit measurements. The full joint detection scheme relies on leveraging both photonic and trapped-ion-based information, each of which has been explored in depth [35–38] and will be addressed next.

A. BPQM decoding

To decode laser communication messages with BPQM, we first present the specific implementation of the algorithm. The photonic input states, namely, BPSK coherent states $|\pm\beta\rangle$,

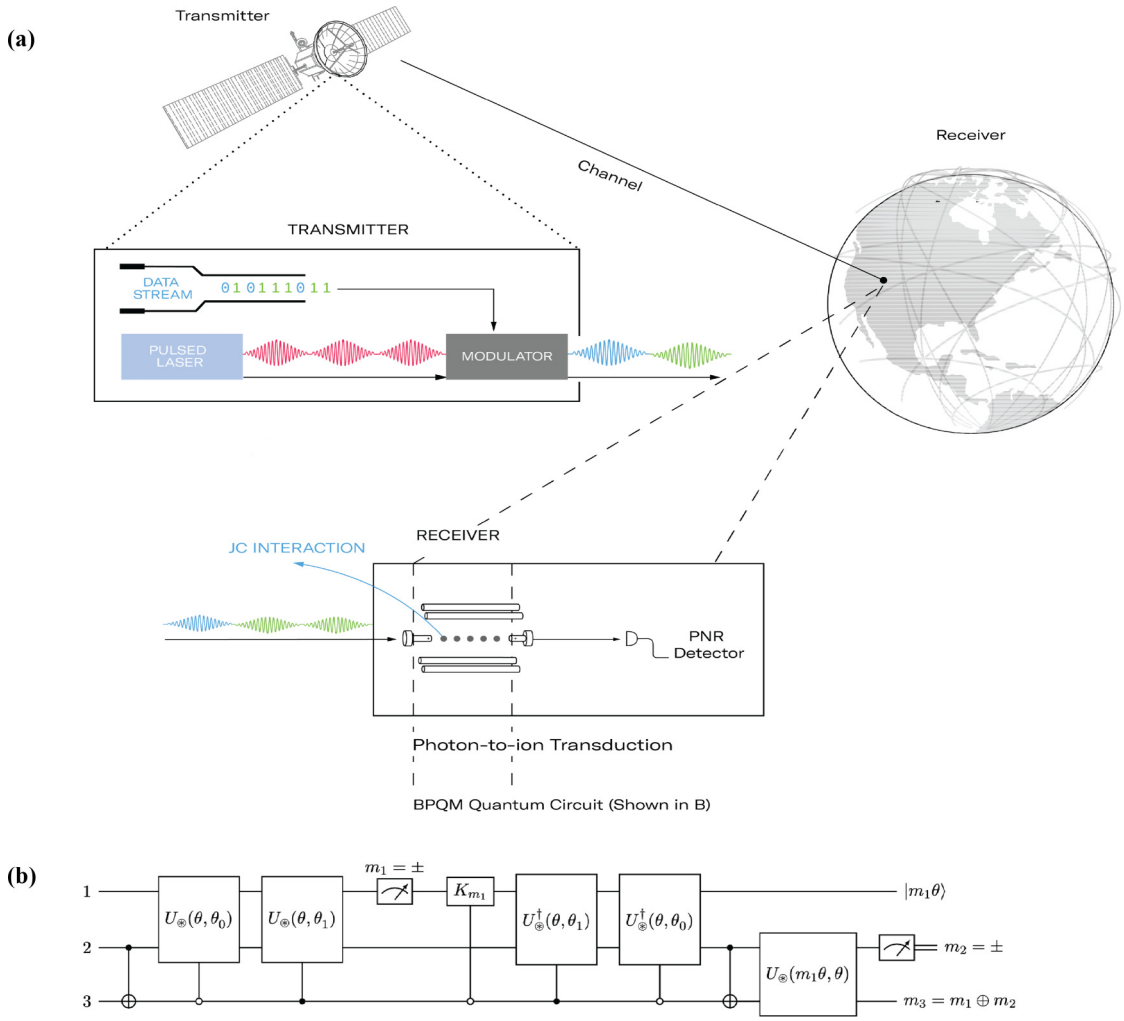

FIG. 1. The schematic and operation of the quantum joint detection receiver for decoding a 3-bit laser-modulated code. (a) The encoded photonic information is efficiently decoded using a trapped-ion quantum computer, which executes (b) the 3-qubit BPQM algorithm circuit. Notation and circuit structure are discussed in the Appendix.

are represented as qubit states $|\pm\theta\rangle$ by the mapping

$$|\pm\beta\rangle \to |\pm\theta\rangle \equiv \cos\left(\frac{\theta}{2}\right)|0\rangle \pm \sin\left(\frac{\theta}{2}\right)|1\rangle, \qquad (1)$$

such that $\sigma = \langle+\beta|-\beta\rangle = \langle+\theta|-\theta\rangle = \cos\theta \neq 0$. The task is to find an efficient decoding algorithm that can discriminate code words constructed using the alphabet defined by these nonorthogonal quantum states. The decoder based on the BPQM algorithm [24] was recently analyzed by Rengaswamy *et al.* [25] for a 5-bit linear tree code, where in noiseless simulations it was shown to surpass the classical bound for decoding error rates at low mean photon numbers. This was followed by a quantum gate decomposition for the various unitary operators described, which provides a starting point for implementation on a real device. These quantum gates effectively perform belief propagation by combining the beliefs at the nodes of the factor graph of the code before iteratively passing on the updated beliefs until the message is jointly decoded, just as in the classical belief-propagation algorithm. The difference here is the leveraging of the quantum regime, where the decoder passes quantum "beliefs" and jointly processes the quantum information present in the symbols before measuring them individually. This allows us to bypass the inevitable loss of information that comes from measuring the individual symbols first, followed by processing the detection outcomes classically. For an example three-bit code $\mathcal{C}$, we arrive at the circuit for the BPQM-based decoder based on the development in Ref. [25], shown in Fig. 1(b). Further description of the code $\mathcal{C}$ and the implementation of the BPQM algorithm for the decoder can be found in the Appendix.

B. Photon-to-ion transduction

Mapping the binary BPSK coherent-state alphabet onto one of two single-qubit states—henceforth called the transduction step—is necessary to fully realize the joint detection receiver. In this step, it is essential that the inner product between the nonorthogonal binary states of the qubits remain the same as that of the received coherent states (under ideal conditions). For coherent states $|\pm\alpha\rangle$ transmitted over a lossy channel of transmissivity η, the received states are $|\pm\beta\rangle = |\pm\sqrt{\eta}\alpha\rangle$ with an overlap of

$$\langle+\beta|-\beta\rangle = e^{-2|\beta|^2} = e^{-2\eta|\alpha|^2} = e^{-2N}, \qquad (2)$$

with N being the received mean photon number. Below we outline a process of performing the aforementioned transduction using the simple and experimentally realizable Jaynes-Cummings interaction between a qubit and a single bosonic mode [39,40].

Based on prior results from [41], we can start by writing down the product state of a single-photon mode and a two-level atom (a trapped ion for our purposes), where the photon mode has been initialized in one of the two coherent states

$$|\pm\beta\rangle = \sum_n e^{-|\beta|^2/2}\frac{(\pm\beta)^n}{\sqrt{n!}}|n\rangle, \tag{3}$$

the atom is initialized in its ground state $|0\rangle$, and the two evolve with the following time-dependent Hamiltonian:

$$H = \hbar\Omega(t)(\sigma_+ a + \sigma_- a^\dagger). \tag{4}$$

Here $\sigma_\pm$ are the raising and lowering operators for the trapped-ion qubit, and a and $a^\dagger$ are photon creation and annihilation operators. Time evolving the initial product state with the above Hamiltonian, we get the following entangled state:

$$|\Psi^\pm(t)\rangle = \sum_n [\cos(\Phi\sqrt{n})\beta_n^\pm|0,n\rangle - i\sin(\Phi\sqrt{n+1})\beta_{n+1}^\pm|1,n\rangle], \tag{5}$$

where

$$\Phi(t) = \int_0^t dt'\Omega(t') \tag{6}$$

and

$$\beta_n^\pm = e^{-|\beta|^2/2}\frac{(\pm\beta)^n}{\sqrt{n!}}. \tag{7}$$

Since this time evolution is unitary, one can verify that the state remains normalized. We now perform a projective measurement on the photon in order to obtain the desired qubit state. The inner product of the two binary qubit states after will depend on the photon measurement result. Since $n=0$ is the most likely measurement outcome, we will ultimately tailor the interaction Ω accordingly, so that an $n=0$ measurement heralds a successful transduction. The probability of achieving an $n=0$ measurement result can be expressed as

$$P(n=0) = e^{-|\beta|^2}[1+\sin^2\Phi(t)\beta^2], \tag{8}$$

and the resulting normalized state of the qubit will be

$$P|_{n=0}|\Psi^\pm(t)\rangle = \frac{1}{\sqrt{1+\sin^2\Phi(t)\beta^2}}[|0\rangle \mp i\sin\Phi(t)\beta|1\rangle]. \tag{9}$$

For a given β, if we were to pick Φ so that the inner products of the optical BPSK states match those of the posttransduction states of the trapped-ion qubit, we would need to satisfy

$$[\langle\Psi^-(t)|P|_{n=0}]P|_{n=0}|\Psi^+(t)\rangle = \langle-\beta|\beta\rangle = e^{-2|\beta|^2}, \tag{10}$$

which would imply the following must hold:

$$\sin\Phi = \frac{1}{\beta}\sqrt{\tanh|\beta|^2}. \tag{11}$$

Thus, we can tailor the time-dependent interaction $\Omega(t)$ so that its integral Φ satisfies the above relation [42]. Plugging this condition into the $n=0$ measurement probability, we can compute the probability of a successful transduction (not accounting for noise) to be as follows:

$$P(n=0) = e^{-|\beta|^2}(1+\tanh|\beta|^2) = e^{-\eta|\alpha|^2}[1+\tanh(\eta|\alpha|^2)]. \tag{12}$$

Note that when $\eta \ll 1$, the above probability decreases very slowly with the transmitted coherent amplitude α since measuring $n=0$ will be highly probable.

With the inclusion of the transduction step, the overall average probability of successful discrimination of the BPSK alphabet binary coherent states is given by the probability that the $n=0$ outcome occurs in the transduction step (heralding probability of successful transduction), multiplied by the maximum success probability of discriminating the two nonorthogonal qubit states within the trapped-ion quantum computer given by $1-P_{e,\min}$, where $P_{e,\min}$ is the Helstrom limit associated with the error probability of discriminating the transduced qubit states (here we assume that the quantum gates and measurements on that trapped-ion qubit are perfect). Thus, the overall average error probability is most generally

$$P_{\text{error}} = 1 - P(n=0)(1-P_{e,\min}) \tag{13}$$

$$= 1 - \frac{e^{-|\beta|^2}}{2}[1+\sin^2\Phi(t)\beta^2] \times\left[1+\sqrt{1-\frac{[1-\sin^2\Phi(t)\beta^2]^2}{[1+\sin^2\Phi(t)\beta^2]^2}}\right]. \tag{14}$$

For a Φ chosen according to Eq. (11), P_{error} in Eq. (14) corresponds to the discrimination error probability associated with an inner-product-preserving transduction step.

If we relax the requirement to preserve the inner product before and after transduction, we can obtain even better performance of overall discrimination of the BPSK coherent-state alphabet states. By controlling the interaction time, and hence Φ, we can make the inner product of the transduced states smaller than that of the optical BPSK states, which increases the heralded success probability of state discrimination in the ion domain. But this comes at the cost of a smaller heralding probability $P(n=0)$, which ensures that the product, i.e., the overall average error probability, remains below the Helstrom limit associated with discriminating the original BPSK binary coherent states. We can minimize P_{error} of Eq. (14) with respect to Φ to find the minimum overall probability of error. The optimal choice of Φ, interestingly, turns out to be not dependent on β, as shown below. The minimum occurs when $\Phi(t) = \frac{\pi}{2}$ and is given by

$$P_{\text{error}} \geqslant 1 - \frac{e^{-|\beta|^2}}{2}(1+|\beta|)^2. \tag{15}$$

For $\Phi = \frac{\pi}{2}$, the inner product of the qubit embeddings of the coherent states is

$$\langle\Psi^-|\Psi^+\rangle = \frac{1-|\beta|^2}{1+|\beta|^2}, \tag{16}$$

which, one can verify, is always smaller than $e^{-2|\beta|^2}$. Despite this, we have actually increased the average probability of

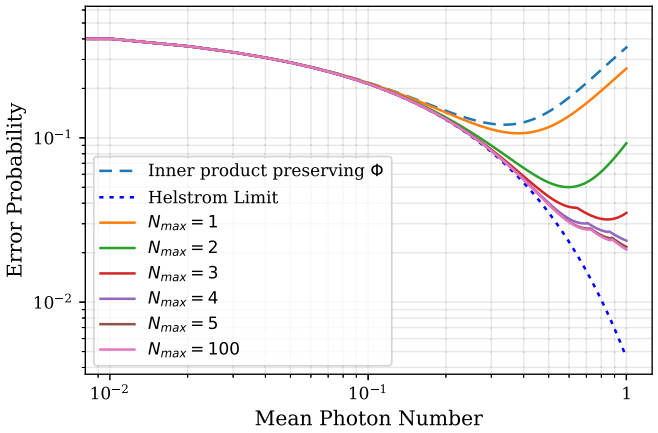

FIG. 2. The single-symbol state discrimination error probability as a function of the received mean photon number. The Helstrom bound (dotted dark blue line) shows the absolute minimum error probability of discriminating the BPSK alphabet binary coherent states in the optical domain, whereas inner-product-preserving Φ (dashed light blue line) and optimized Φ for various points of truncation in the sum in Eq. (17) (solid lines between the dashed and dotted lines corresponding to increasing values of $N_{\max}$) show the overall average error probability of optical BPSK state discrimination, using our receiver. The photon-to-ion transduction step uses two different choices for Φ, e.g., Φ given by Eq. (11) for the inner-product-preserving transduction and $\Phi = \pi/2$ for transduction that results in the optimal overall average error probability when we truncate Eq. (17) after $n = 1$. All of the above assume ideal quantum logic gates and measurements once in the ion domain.

successfully discriminating the coherent-state BPSK alphabet by optimally choosing Φ. The improvement when compared to Φ in Eq. (11), corresponding to inner-product-preserving transduction, is shown in Fig. 2. The Helstrom limit associated with discriminating the original BPSK alphabet binary coherent states is also plotted for comparison. In the following sections we will consider the exact inner-product scenario [Eq. (12)] as our probability of successful transduction, but the above discussion shows that the experimentally obtained performance reported in this paper can improve further only if the optimal Φ is chosen for the transduction step.

If we have photon-number-resolving (PNR) detection available, we can resolve higher (nonzero) values of n, and the average error probability of discriminating the BPSK coherent states attained by our transduction method followed by an ideal trapped-ion quantum processor is given by

$$P_{e,\text{receiver}}(\Phi) = 1 - \frac{1}{2}\sum_n P_n(\Phi)\left[1 + \sqrt{1-\sigma_n^2}\right], \qquad (17)$$

which, as before, can be minimized by optimally choosing Φ. Above, σ_n is the inner product between the two possible ion states heralded by a measurement of n photons, which is

$$\sigma_n = \frac{\cos^2(\sqrt{n}\Phi) - \frac{\beta^2}{n+1}\sin^2(\sqrt{n+1}\Phi)}{\cos^2(\sqrt{n}\Phi) + \frac{\beta^2}{n+1}\sin^2(\sqrt{n+1}\Phi)}. \qquad (18)$$

Although the terms in the sum are rather complicated, for a given value of β, one can easily numerically minimize the above function and include arbitrarily many terms. This has been done for several different levels of series truncation in Fig. 2. This would ensure optimized performance assuming the availability of PNR detection.

III. BPQM ON THE HONEYWELL LT-1.0 TRAPPED-ION PROCESSOR

Next, we present the demonstration of the BPQM algorithm on a recently developed quantum device. The implementation on a currently available quantum processing unit provides a performance standard and outlook for these joint detection receivers based on the scheme set forth in this work. For this experiment, we utilized the Honeywell LT-1.0 trapped-ion device, which uses ^{171}Yb+ ions. The choice of the device was motivated by the unique combination of high-fidelity quantum gates, all-to-all qubit connectivity afforded by trapped-ion architecture, and the unique capability to perform midcircuit measurements on selected qubits to condition subsequent gate operations on their measurement outcomes. The all-to-all connectivity enables a number of circuit optimizations that allow the avoidance of costly SWAP gates, resulting in the compact decomposition of the circuit depicted in Fig. 1(b), which requires 81 two-qubit Mølmer-Sørenson-like ZZ gates [43]. In the absence of a physical implementation of the photon-to-ion transduction, the initial states of the qubits are prepared directly based on the chosen code word for every given run rather than created as a result of the photon projective measurement. With the exception of the noisy simulation, the data points were taken assuming lossless transduction. While the proposed transduction scheme has not been exactly experimentally implemented, the Jaynes-Cummings coupling already serves as a reasonable model of the laser-ion interaction in current trapped-ion devices [44], making it a highly possible near-term development.

As a first step, we look at decoding only the first bit of the full code word. For this we are able to use an abbreviated version of the circuit that is truncated at the first measurement on the top qubit. This gives us an estimate of how the decoder and the $U_\circledast$ unitary gates are performing on the device without immediately evaluating the longer gate depth of the full decoder. This significantly reduces the gate count, allowing us to exceed the classical bound for a range of low received mean photon numbers, shown in Fig. 3(a). While this demonstration shows relatively modest improvements when compared to classical approaches, these points give us confidence in the implementation of the $U_\circledast$ blocks and allow us to move forward to the full circuit.

In the full decoder circuit, the code-word output is determined by both the intermediate and final measurements. This circuit gives us an accurate look at the performance of BPQM on current devices. Noiseless simulations are shown to beat the classical bound for error probability of decoding over a range of low mean photon numbers for values within the Moon to Mars downlink regime in Fig. 3(b). On the other hand, running the circuit on hardware produces a curve that trends at and peeks below the classical bound at very low mean photon numbers, presenting a quantum advantage. We note that the hardware curve shows anomalous behavior with increasing mean photon number, where it trends worse than the classical bound. This is due to the infidelities associated

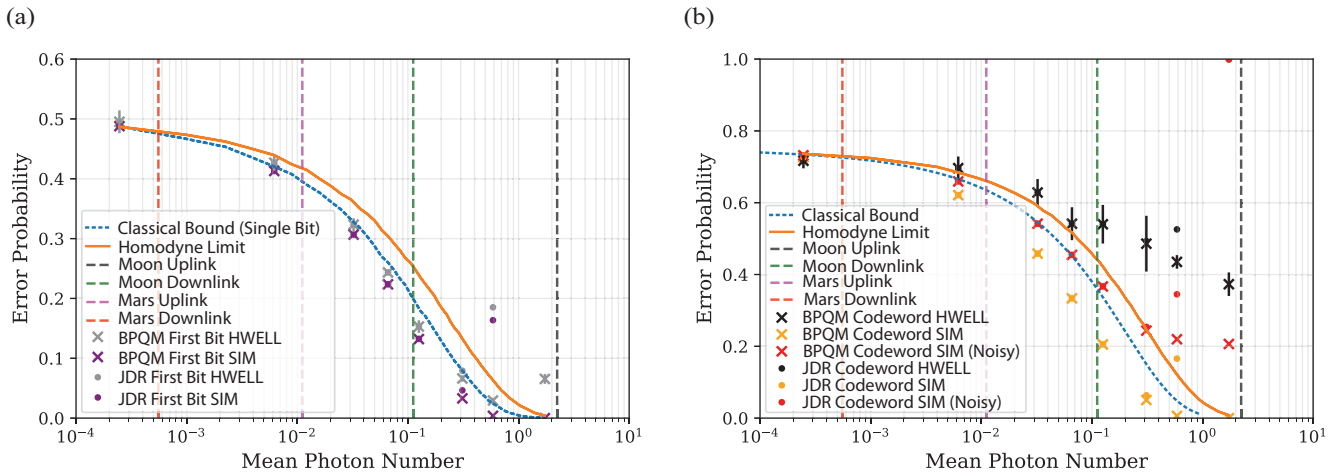

FIG. 3. Experimental results for (a) the first-bit and (b) full 3-bit decoder with four code words, with 1000 and 512 shots per run, respectively. The "classical" bound represents the error probability associated with measuring the individual symbols in the photonic domain sans the trapped-ion receiver using the quantum-optimal Helstrom measurement followed by classical maximum-likelihood decoding (dotted blue line). The Homodyne limit corresponds to a practical classical bound, where the Helstrom measurements are replaced by homodyne measurements (solid orange line). "BPQM" points represent circuit runs as is with perfect transduction assumed, whereas "JDR" points account for the probability of successful transduction based on our scheme [the cube of Eq. (12) in (b), to account for three qubits]. Experimental error probabilities of decoding with the trapped-ion receiver (gray crosses, first bit; black crosses, full decoder) are averaged over four code words, with error bars for standard deviation. Noiseless (purple crosses for the first bit, yellow crosses for the full decoder) and noisy (red crosses) simulation results are shown for comparison. The dashed vertical lines denote typical values for the mean photon numbers associated with Moon uplink, Moon downlink, Mars uplink, and Mars downlink (right to left, respectively).

with initializing the trapped-ion qubits in states $|\pm\theta\rangle$, corresponding to large coherent amplitudes β in states $|\pm\beta\rangle$. Additionally, the "JDR" points diverge from the "BPQM" points as the mean photon number becomes larger due to a rapidly decreasing probability of successful transduction. However, when we consider the advantage scenario of low mean photon numbers, our noisy simulations to find the operating fidelities of one- and two-qubit depolarizing errors that can bring us to the classical bound show a "checkpoint" that can drive future experimental pushes. This is shown in Fig. 3(b) along with the experimental data. We consider a simple depolarizing error model with one- and two-qubit depolarizing noises set to 0.0001 and 0.005, respectively, while the photonic input state preparation was given a 0.0001% fail rate based on values of Jaynes-Cummings error rates within existing ion traps being approximately equivalent to a single-qubit gate. This checkpoint is intended to be viewed as a more general noise level regime rather than a specific benchmark, but it shows a clear path toward achieving fully useful quantum advantage in the low-photon-number regime. It is thus clear that the BPQM algorithm is mainly limited by gate fidelity in achieving a lower error probability for decoding messages for the types of channels highlighted.

Of particular interest in Fig. 3 is the projected mean photon number corresponding to lunar and future Mars links based on the specifications of optical elements used in NASA's 2013 Lunar Laser Communication Demonstration [2] experiment. For example, the Mars uplink corresponds to a received mean photon number per pulse of 10^{-2}. Notably, at this mean photon number, the BPQM-based receiver ideally surpasses the classical limit in the average error probability of decoding the codes of the example 3-bit code by approximately 2%–3%. At the same mean photon number, by choosing a different code—one that achieves the Holevo capacity—it would be possible to reliably communicate at rates 5 times the best possible rate for communication with classical decoders, as depicted in Fig. 4. Note that the capacities plotted in Fig. 4 are the Holevo capacities of the end-to-end channel between the sender and the receiver subject to the probabilistic photon-to-ion transduction. These are still better rates for all links except the Moon uplink due to its higher mean photon number and thus low $P(n = 0)$.

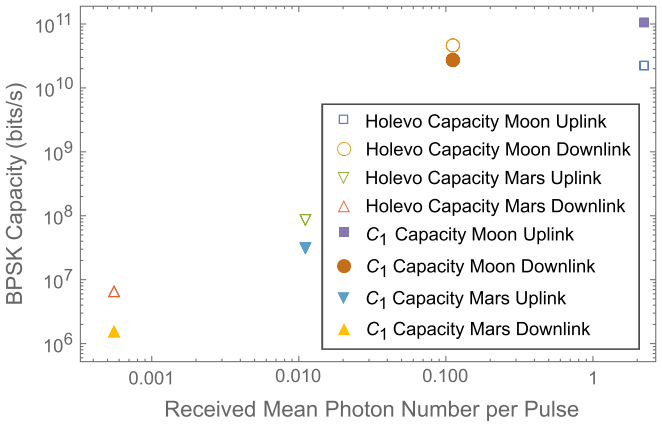

FIG. 4. Link budgets based on LLC specs for an uplink and downlink. The Holevo capacities plotted here denote the quantum bound for classical communication capacity using joint detection of symbols via probabilistic photon-to-ion transduction. The C_1 capacities are the capacities associated with symbol-by-symbol optical detection for the BPSK scheme at the given link distances.

IV. CONCLUSIONS AND OUTLOOK

Here we conclusively realized a previously postulated joint quantum detection scheme on a trapped-ion quantum device and showed an experimental framework to surpass the quantum limit on the minimum average decoding error probability in the low-photon limit. By leveraging a combination of midcircuit measurement-enabled experiments, the connectivity of trapped-ion devices, and a mapping of the relevant photonic coherent states onto inner-product-preserving single-qubit states, our work shows a quantum joint detection receiver for a 3-bit BPSK modulated linear tree code using the BPQM algorithm. Continued reduction of trapped-ion device error rates—particularly two-qubit gate infidelities and midcircuit measurement-induced cross-talk error rates—will push the noise boundary such that future experiments of this scheme can reliably exceed the classical bound for low photon numbers. Further, as gate fidelities improve, the postmeasurement error-mitigation techniques and gate-decomposition optimizations presented here will give us a distinct path towards exceeding the classical bound for decoding in general joint detection schemes with a larger codebook. Note that we considered purely lossy optical transmissions, whereas in practice there will also be additional thermal noise. For such more realistic scenarios, the extent of quantum advantage that is possible with joint detection schemes over the corresponding classical bound for decoding is expected to be further diminished, which in turn pushes the bar on gate fidelities higher. However, for optical-frequency free-space communications, even at daytime temperatures, the Planck-law-limited thermal noise is below 10^{-5} mean photons per mode, which is in a regime where the results of our pure-loss-channel analysis are fairly accurate.

The joint detection receiver protocol shown here provides additional impetus for the development of photonic transduction in trapped-ion hardware in the near future. Photonic interconnects are already under development for the purpose of constructing modular trapped-ion architectures [38,45], and the basic functionality can, in principle, be extended to connect a trapped-ion device to a photonic quantum device. Regardless, photon-to-ion transduction will be an essential feature of any technological realization of BPQM. Finally, we highlight the promise of such schemes for deep-space communications and upcoming space missions, a dedicated Mars link, and advances in astronomy.

ACKNOWLEDGMENTS

This work is supported by Air Force STTR Grants No. FA8750-20-P-1721 and No. FA8750-20-P-1704. K.P.S. and S.G. acknowledge support from the National Science Foundation (NSF) project "CIF: Medium: Iterative Quantum LDPC Decoders," Award No. 1855879, and the Office of Naval Research (ONR) MURI project on "Optical Computing," Grant No. N00014-14-1-0505. K.P.S. acknowledges NSF Grant No. 2204985. The authors gratefully acknowledge the entire Honeywell Quantum Solutions team, especially Dr. B. Neyenhuis, for helpful discussions and support in running these experiments. The authors thank Dr. M. Fanto (AFRL) as well as S. Willis and Dr. N. Aggarwal (Aliro Technologies) for helpful feedback on the work and manuscript. K.P.S. thanks Dr. N. Rengaswamy for helpful discussions.

S.G. suggested the idea underlying this project. P.N. and S.G. codirected the project. C.D. and K.P.S. jointly worked on the theory and BPQM circuits with midcircuit measurements. I.M., C.D., and P.N. jointly worked on the photon-ion step. C.D., I.M., and A.G. jointly performed all the experiments presented here. All authors contributed to the analysis and writing of the manuscript.

The authors declare no competing interests.

APPENDIX: METHODS

1. BPQM

The factor graph defining the 3-bit code considered in this paper is

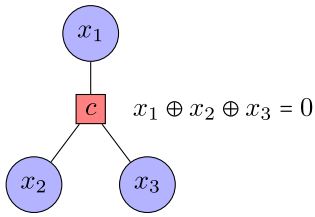

(A1)

which generates the set of code words

$$\mathcal{C} = \{000, 110, 101, 011\}. \tag{A2}$$

The gates used for message combining at the check nodes and bit nodes of the factor graph are the controlled-NOT (CNOT) gate and a unitary $U_{\circledast}$, given by

$$U_{\circledast}(\theta, \theta') = \begin{pmatrix} a_+ & 0 & 0 & a_- \\ a_- & 0 & 0 & -a_+ \\ 0 & b_+ & b_- & 0 \\ 0 & b_- & -b_+ & 0 \end{pmatrix}, \tag{A3}$$

where

$$a_\pm = \frac{1}{\sqrt{2}} \frac{\cos\left(\frac{\theta-\theta'}{2}\right) \pm \cos\left(\frac{\theta+\theta'}{2}\right)}{\sqrt{1+\cos\theta\cos\theta'}}, \tag{A4}$$

$$b_\pm = \frac{1}{\sqrt{2}} \frac{\sin\left(\frac{\theta+\theta'}{2}\right) \mp \sin\left(\frac{\theta-\theta'}{2}\right)}{\sqrt{1-\cos\theta\cos\theta'}}, \tag{A5}$$

$$\cos\theta_0 = \frac{\cos\theta + \cos\theta'}{1+\cos\theta\cos\theta'}, \cos\theta_1 = \frac{\cos\theta - \cos\theta'}{1-\cos\theta\cos\theta'}. \tag{A6}$$

In the above equations, θ captures the angle of the input qubits and can be translated to the mean photon number N by the relation $e^{-2N} = \cos\theta$. In essence, this $U_{\circledast}$ unitary compresses the information of the two qubits into one, leaving the other in a fixed state, the $|0\rangle$ state. For more details, refer to [24,25].

2. Classical limits

When decoding the first bit alone, the ideal classical bound corresponds to performing the pulse-by-pulse detection based on the quantum-optimal Helstrom measurement, followed by inference of the bit using the classical belief propagation algorithm. Since the code has a tree factor graph, classical belief propagation amounts to maximum-likelihood decoding. Likewise, the practical classical bound also corresponds to

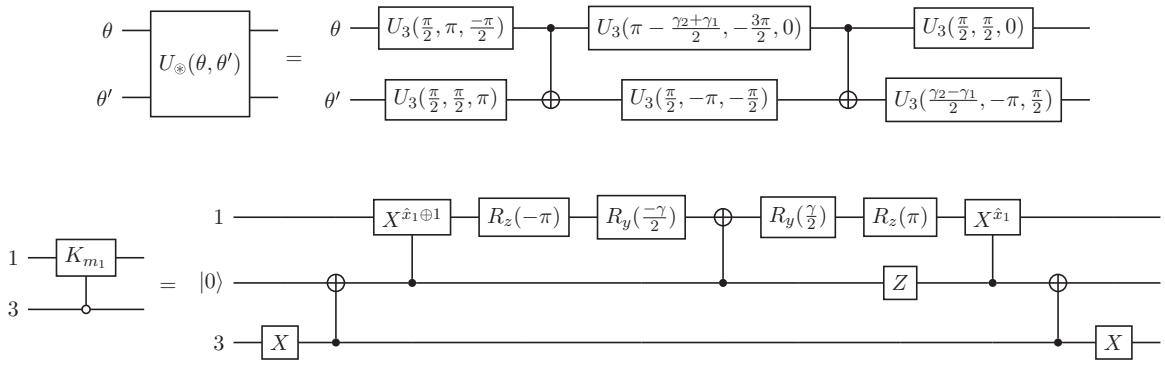

FIG. 5. Both decompositions for BPQM full decoder components. (a) U gate decomposition, where U_3 is the QISKIT rotation gate and γ_1 and γ_2 are defined in Eq. (A9). (b) K_m gate decomposition, utilizing ancilla qubit 3.

pulse-by-pulse detection, except where the Helstrom measurement is replaced by coherent homodyne detection. The relevant pulse-by-pulse discriminating measurement average error probabilities are given by

$$p_{\text{Hel}} = \tfrac{1}{2}(1-\sin\theta),$$
$$p_{\text{Homodyne}} = \tfrac{1}{2}\operatorname{erfc}\sqrt{-\ln\cos\theta}, \quad \theta\in(0,\pi/2). \tag{A7}$$

For the full decoder circuit, the classical bound is the average error probability associated with code-word maximum-likelihood detection following either pulse-by-pulse Helstrom (ideal) or homodyne (practical) measurements.

3. Quantum limits

A lower bound on the quantum-enhanced classical communication capacity with the trapped-ion joint detection receiver following photonic-to-ionic transduction is given by considering the classical-input–quantum-output (cq) channel analog of the "channel with random state" classical channel model, as defined in [46]. The latter is defined as a discrete memoryless channel with state $(\mathcal{X},\mathcal{S},p(y|x,s),\mathcal{Y})$, with $\mathcal{X},\mathcal{Y},\mathcal{S}$ denoting the input-, output-, and channel-state alphabets, respectively (assumed to be finite), where the channel-state sequence $\{S_i\}$ is an independent and identically distributed (i.i.d.) process with distribution $P_S(s)$, i.e., changing randomly for every use of the channel. For such a channel, there are many possible scenarios with respect to the availability of the state information to the encoder and the decoder. The scenario that is relevant to us here is the one where the information about the state sequence is available only at the decoder. In this case, the capacity is given by $C=\max_p(x)I(X;Y|S)$. The achievability part follows trivially from treating (Y^n,S^n) as the output of the channel $p(y,s|x)=p(s)p(y|x,s)$. The achievability remains good also when the channel output Y is quantum, i.e., for a cq channel with random channel state, where the channel state is known only to the decoder. Thus, a lower bound on the achievable capacity for BPSK communications with a trapped-ion joint detection receiver is

$$R = P_{n=0}\times h_2\left(\frac{1+e^{-2\eta|\alpha|^2}}{2}\right), \tag{A8}$$

where $P_{n=0}$ is the transduction success probability, η is the transmissivity of the channel, and $|\alpha|$ is the amplitude of the transmitted laser pulse. This value is plotted in Fig. 4 after calculating $P_{n=0}$ for the photon-to-ion transduction mechanism discussed in the main text. We note that the converse part of the coding theorem for the cq channel remains open.

4. Link budgets

To describe the various link values for practical application, we calculated mean-photon-number values based on specs from the 2013 NASA Lunar Laser Communications Demonstration, i.e., laser wavelength (1.6 μm), dimensions of telescopes (0.1 m on the Moon and Mars and 0.4 m on Earth diameters), and laser powers (10-W uplink and 0.5-W downlink). Additionally, we assume a modulation bandwidth of (a) $\tau = 10$ ps, i.e., a 100-GHz laser source, for the Moon and (b) $\tau = 1$ ns, i.e., a 1-GHz pulsed laser source, for Mars.

5. Circuit definitions and optimizations

For the first bit decoding in the circuit, it is equivalent to conditionally applying the two $U_{\circledast}$ gates based on a midcircuit measurement on the third qubit following the initial CNOT gate. This avoids the trouble of decomposing $CU_{\circledast}$ into native two-qubit gates, and we can simply use $U_{\circledast}$ itself, thanks to the midcircuit measurement capabilities of the Honeywell device. The resulting circuits have only six two-qubit gates. It is important to note that although each individual point's circuits were run back to back, all points were not collected during the same device session. Gate fidelities can drift from day to day on the same device but not enough to significantly impact our results.

For the full decoder circuit, the $U_{\circledast}$ unitary was constructed by taking its components and adding a control line onto each gate, with the components shown in Fig. 5(a), where

$$\gamma_1 = 2\sin^{-1}(a_-),\ \gamma_2 = 2\sin^{-1}(b_+). \tag{A9}$$

These circuit components were optimized through QISKIT's transpilation function and various pencil-and-paper optimizations, which produced a slightly different structure than the original implementation shown in [25]. K_{m_1} is given in Fig. 5(b) and was applied as shown. The midcircuit measurement on the first qubit required an active qubit reset to

avoid drifting into a noncomputational subspace, and all measurements were performed in the X basis. The final circuits with a two-qubit gate count of 81 were submitted to the Honeywell device via an application programming interface (API) call to the Honeywell system in quantum assembly language (QASM) form. Decomposition to native gates and qubit gate specifics were handled by Honeywell's internal software. Honeywell qubits are shuttled between various gate zones, which gives effective all-to-all connectivity. See their release paper [47] for specifics.

[1] L. J. Deutsch, Towards deep space optical communications, Nat. Astron. **4**, 907 (2020).

[2] D. M. Boroson, B. S. Robinson, D. V. Murphy, D. A. Burianek, F. Khatri, J. M. Kovalik, Z. Sodnik, and D. M. Cornwell, Overview and results of the lunar laser communication demonstration, Proc. SPIE **8971**, 89710S (2014).

[3] C. Gerry and P. Knight, *Introductory Quantum Optics* (Cambridge University Press, Cambridge, 2004).

[4] C. W. Helstrom, Quantum detection and estimation theory, J. Stat. Phys. **1**, 231 (1969).

[5] S. J. Dolinar, A class of optical receivers using optical feedback, Ph.D. thesis, Massachusetts Institute of Technology, 1976.

[6] J. Chen, J. L. Habif, Z. Dutton, R. Lazarus, and S. Guha, Optical codeword demodulation with error rates below the standard quantum limit using a conditional nulling receiver, Nat. Photonics **6**, 374 (2012).

[7] F. E. Becerra, J. Fan, G. Baumgartner, J. Goldhar, J. T. Kosloski, and A. Migdall, Experimental demonstration of a receiver beating the standard quantum limit for multiple nonorthogonal state discrimination, Nat. Photonics **7**, 147 (2013).

[8] F. E. Becerra, J. Fan, and A. Migdall, Photon number resolution enables quantum receiver for realistic coherent optical communications, Nat. Photonics **9**, 48 (2015).

[9] R. Nair, S. Guha, and S.-H. Tan, Realizable receivers for discriminating coherent and multicopy quantum states near the quantum limit, Phys. Rev. A **89**, 032318 (2014).

[10] S. J. Dolinar, Jet Propulsion Laboratory, A near-optimum receiver structure for the detection of M-ary optical PPM signals, TDA Progress Report No. 42, 1983 (unpublished), https://ipnpr.jpl.nasa.gov/progress_report/42-72/72C.PDF.

[11] S. Guha, J. L. Habif, and M. Takeoka, Approaching Helstrom limits to optical pulse-position demodulation using single photon detection and optical feedback, J. Mod. Opt. **58**, 257 (2011).

[12] R. S. Bondurant, Near-quantum optimum receivers for the phase-quadrature coherent-state channel, Opt. Lett. **18**, 1896 (1993).

[13] M. P. da Silva, S. Guha, and Z. Dutton, Achieving minimum-error discrimination of an arbitrary set of laser-light pulses, Phys. Rev. A **87**, 052320 (2013).

[14] A. S. Holevo, The capacity of the quantum channel with general signal states, IEEE Trans. Inf. Theory **44**, 269 (1998).

[15] B. Schumacher and M. D. Westmoreland, Sending classical information via noisy quantum channels, Phys. Rev. A **56**, 131 (1997).

[16] V. Giovannetti, S. Guha, S. Lloyd, L. Maccone, J. H. Shapiro, and H. P. Yuen, Classical Capacity of the Lossy Bosonic Channel: The Exact Solution, Phys. Rev. Lett. **92**, 027902 (2004).

[17] V. Giovannetti, R. García-Patrón, N. J. Cerf, and A. S. Holevo, Ultimate classical communication rates of quantum optical channels, Nat. Photonics **8**, 796 (2014).

[18] H. W. Chung, S. Guha, and L. Zheng, Superadditivity of quantum channel coding rate with finite blocklength joint measurements, IEEE Trans. Inf. Theory **62**, 5938 (2016).

[19] Z. Dutton, S. Guha, J. Chen, and J. L. Habif, Superadditive optical communications with joint detection receivers and concatenated coding, *Frontiers in Optics 2011/Laser Science XXVII*, (Optica Publishing Group, 2011), p. LTuI5.

[20] S. Guha, Z. Dutton, and J. H. Shapiro, On quantum limit of optical communications: Concatenated codes and joint-detection receivers, in *Proceedings of the 2011 IEEE International Symposium on Information Theory Proceedings* (IEEE, Piscataway, NJ, 2011), pp. 274–278.

[21] M. Takeoka and S. Guha, Capacity of optical communication in loss and noise with general quantum gaussian receivers, Phys. Rev. A **89**, 042309 (2014).

[22] S. Guha, Structured Optical Receivers to Attain Superadditive Capacity and the Holevo Limit, Phys. Rev. Lett. **106**, 240502 (2011).

[23] M. M. Wilde and S. Guha, Polar codes for classical-quantum channels, IEEE Trans. Inf. Theory **59**, 1175 (2013).

[24] J. M. Renes, Belief propagation decoding of quantum channels by passing quantum messages, New J. Phys. **19**, 072001 (2017).

[25] N. Rengaswamy, K. P. Seshadreesan, S. Guha, and H. D. Pfister, Quantum-message-passing receiver for quantum-enhanced classical communications, npj Quantum Inf. **7**, 97 (2021).

[26] N. Rengaswamy, K. P. Seshadreesan, S. Guha, and H. D. Pfister, Quantum advantage via qubit belief propagation, in *Proceedings of the 2020 IEEE International Symposium on Information Theory (ISIT)* (IEEE, Piscataway, NJ, 2020), pp. 1824–1829.

[27] K. Wright *et al.*, Benchmarking an 11-qubit quantum computer, Nat. Commun. **10**, 5464 (2019).

[28] K. Head-Marsden, J. Flick, C. J. Ciccarino, and P. Narang, Quantum information and algorithms for correlated quantum matter, Chem. Rev. **121**, 3061 (2016).

[29] S. Debnath, N. M. Linke, C. Figgatt, K. A. Landsman, K. Wright, and C. Monroe, Demonstration of a small programmable quantum computer with atomic qubits, Nature (London) **536**, 63 (2016).

[30] T. Monz, D. Nigg, E. A. Martinez, M. F. Brandl, P. Schindler, R. Rines, S. X. Wang, I. L. Chuang, and R. Blatt, Realization of a scalable Shor algorithm, Science **351**, 1068 (2016).

[31] J. T. Barreiro, M. Müller, P. Schindler, D. Nigg, T. Monz, M. Chwalla, M. Hennrich, C. F. Roos, P. Zoller, and R. Blatt, An open-system quantum simulator with trapped ions, Nature (London) **470**, 486 (2011).

[32] S. Gulde, M. Riebe, G. P. T. Lancaster, C. Becher, J. Eschner, H. Häffner, F. Schmidt-Kaler, I. L. Chuang, and R. Blatt, Implementation of the Deutsch–Jozsa algorithm on an ion-trap quantum computer, Nature (London) **421**, 48 (2003).

[33] S. Muralidharan, J. Kim, N. Lütkenhaus, M. D. Lukin, and L. Jiang, Ultrafast and Fault-Tolerant Quantum Communication across Long Distances, Phys. Rev. Lett. **112**, 250501 (2014).

[34] S. Muralidharan, L. Li, J. Kim, N. Lütkenhaus, M. D. Lukin, and L. Jiang, Optimal architectures for long distance quantum communication, Sci. Rep. **6**, 20463 (2016).

[35] S. Pirandola, J. Eisert, C. Weedbrook, A. Furusawa, and S. L. Braunstein, Advances in quantum teleportation, Nat. Photonics **9**, 641 (2015).

[36] B. B. Blinov, D. L. Moehring, L. M. Duan, and C. Monroe, Observation of entanglement between a single trapped atom and a single photon, Nature (London) **428**, 153 (2004).

[37] D. Hucul, I. V. Inlek, G. Vittorini, C. Crocker, S. Debnath, S. M. Clark, and C. Monroe, Modular entanglement of atomic qubits using photons and phonons, Nat. Phys. **11**, 37 (2015).

[38] C. Monroe, R. Raussendorf, A. Ruthven, K. R. Brown, P. Maunz, L.-M. Duan, and J. Kim, Large-scale modular quantum-computer architecture with atomic memory and photonic interconnects, Phys. Rev. A **89**, 022317 (2014).

[39] W. Vogel and R. L. de Matos Filho, Nonlinear Jaynes-Cummings dynamics of a trapped ion, Phys. Rev. A **52**, 4214 (1995).

[40] D. Leibfried, R. Blatt, C. Monroe, and D. Wineland, Quantum dynamics of single trapped ions, Rev. Mod. Phys. **75**, 281 (2003).

[41] R. Han, J. A. Bergou, and G. Leuchs, Near optimal discrimination of binary coherent signals via atom-light interaction, New J. Phys. **20**, 043005 (2018).

[42] B. M. Rodríguez-Lara, H. Moya-Cessa, and A. B. Klimov, Combining Jaynes-Cummings and anti-Jaynes-Cummings dynamics in a trapped-ion system driven by a laser, Phys. Rev. A **71**, 023811 (2005).

[43] K. Mølmer and A. Sørensen, Multiparticle Entanglement of Hot Trapped Ions, Phys. Rev. Lett. **82**, 1835 (1999).

[44] S. Haroche, Nobel lecture: Controlling photons in a box and exploring the quantum to classical boundary, Rev. Mod. Phys. **85**, 1083 (2013).

[45] R. R. C. Monroe and J. Kim, Fault tolerant scalable modular quantum computer architecture with an enhanced control of multi-mode couplings between trapped ion qubits, US Patent No. 9858531B1 (2 January 2018).

[46] A. A. El Gamal and Y.-H. Kim, *Network Information Theory* (Cambridge University Press, Cambridge, 2018).

[47] J. M. Pino, J. M. Dreiling, C. Figgatt, J. P. Gaebler, S. A. Moses, M. S. Allman, C. H. Baldwin, M. Foss-Feig, D. Hayes, K. Mayer, C. Ryan-Anderson, and B. Neyenhuis, Demonstration of the qccd trapped-ion quantum computer architecture, Nature (London) **592**, 209 (2021).